Numerical Simulation of Two-Dimensional Unsteady Transonic Flows Using the Full-Potential Equation

J. B. Malone*
Lockheed-Georgia Company, Marietta, Georgia
and
N. L. Sankar†
Georgia Institute of Technology, Atlanta, Georgia

A numerical procedure is presented for computing the aerodynamic flowfield about airfoils using the two-dimensional, full-potential equation. A strongly implicit approximate factorization algorithm is employed which may be applied either as a relaxation procedure for steady flow problems, or as an accurate noniterative time-marching procedure for unsteady flows. A body-fitted coordinate system which follows the airfoil motion during unsteady computations is used to permit exact application of the appropriate boundary conditions on the instantaneous airfoil surface. Numerical results are presented for steady, unsteady, subsonic, and transonic flows about several different airfoil shapes.

Introduction

THE development and application of supercritical airfoil technology has made feasible the design of transonic-cruise transport aircraft with optimum rigid aircraft aerodynamic performance characteristics.[1] Flight at transonic Mach numbers, however, may be accompanied by a significant decrease in aircraft flutter speed.[2] Unfortunately, the occurrence of this important aeroelastic instability cannot be predicted adequately by extrapolating unsteady subsonic-aerodynamic theory into the transonic regime. Instead, successful transonic flutter analysis methods must incorporate unsteady aerodynamic theories which properly account for shock-wave development and motions. These unsteady transonic-aerodynamic methods must be computationally accurate, reliable, and efficient, in order to confidently predict safe operational limits for transonic-cruise aircraft.

Several groups of researchers have developed solution methods for the two-dimensional, unsteady, full-potential equation. Numerical methods have been developed by Steger and Caradonna,[3] Goorjian,[4] Chipman and Jameson,[5] Sankar and Tassa,[6] Chang,[7] and, most recently, Bridgeman et al.[8]

In this paper, a strongly implicit approximate factorization algorithm is described for solving the steady and unsteady transonic full-potential equation. The new procedure is based on Sankar's earlier, nonconservative two-dimensional, full-potential method.[6] The present numerical method, however, uses a fully conservative formulation that is applied on a moving, body-fitted coordinate system. A useful feature of the present method is that it may be applied either as a relaxation procedure for steady flow problems, or as an accurate noniterative time-marching procedure for unsteady flows.

Received Dec. 27, 1982; presented as Paper 83-0233 at the AIAA 21st Aerospace Sciences Meeting, Reno, Nev., Jan. 10-13, 1983; revision received Nov. 11, 1983.

*Scientist. Member AIAA.
†Senior Research Engineer, School of Aerospace Engineering. Member AIAA.

Mathematical Formulation

Two-dimensional steady and unsteady transonic potential flow problems are governed by the following equations ($\sigma=0$ steady, $\sigma=1$ unsteady).

Conservation of mass:

$$\sigma\rho_t+(\rho\phi_x)_x+(\rho\phi_y)_y=0 \tag{1}$$

Conservation of energy:

$$a_\infty^2+\frac{\gamma-1}{2}V_\infty^2=a^2+\frac{\gamma-1}{2}(\sigma 2\phi_t+\phi_x^2+\phi_y^2) \tag{2}$$

Isentropic gas relationship:

$$\rho=\rho_\infty(a^2/a_\infty^2)^{1/\gamma-1} \tag{3}$$

In these equations, ϕ is the velocity potential, ρ the density, and V_∞ the velocity of the undisturbed fluid at infinity. The local and freestream values of the speed of sound are represented by the quantities a and a_∞, respectively, and γ is the ratio of specific heats.

For convenience in the following analysis, all densities and velocities are nondimensionalized by the corresponding freestream values, ρ_∞ and V_∞. The length scales are nondimensionalized with respect to a reference length c, and the time quantities are similarly scaled by the ratio c/V_∞.

The preceding equations may be recast in a strong conservation form in a coordinate system (ξ,η,τ) which is related to the physical coordinates (x,y,t) by the following general transformation:

$$\xi=\xi(x,y,t):\quad \eta=\eta(x,y,t):\quad \tau=t \tag{4}$$

In this new coordinate system, the equation governing the conservation of mass is given by

$$\sigma\left(\frac{\rho}{J}\right)_\tau+\left(\frac{\rho U}{J}\right)_\xi+\left(\frac{\rho V}{J}\right)_\eta=0 \tag{5}$$

while the fluid density ρ is given by

$$\rho=\left[1+\frac{\gamma-1}{2}M_\infty^2(1-2\sigma\phi_\tau-(U+\xi_t)\phi_\xi-(V+\eta_t)\phi_\eta)\right]^{1/\gamma-1} \tag{6}$$

and M_∞ is the freestream Mach number. The equations below define the required geometric and kinematic quantities in the computational domain.

$$\xi_t = -\sigma(\xi_x x_\tau + \xi_y y_\tau) \tag{7a}$$

$$\eta_t = -\sigma(\eta_x x_\tau + \eta_y y_\tau) \tag{7b}$$

$$U = \xi_t + A_1\phi_\xi + A_2\phi_\eta \tag{7c}$$

$$V = \eta_t + A_2\phi_\xi + A_3\phi_\eta \tag{7d}$$

$$A_1 = \xi_x^2 + \xi_y^2 \tag{7e}$$

$$A_2 = \xi_x\eta_x + \xi_y\eta_y \tag{7f}$$

$$A_3 = \eta_x^2 + \eta_y^2 \tag{7g}$$

$$J = \xi_x\eta_y - \xi_y\eta_x \tag{7h}$$

In the above equations x_τ and y_τ are the Cartesian components of velocity of the time-deforming grid. The quantities U and V are the contravariant components of velocity which are proportional to the components of the relative velocity between the fluid and the grid in the $\nabla\xi$ and $\nabla\eta$ directions, respectively. Also, J is the Jacobian of the transformation and the quantities A_1, A_2, and A_3 are the metrics of transformation.

Equation Discretization and Linearization

An implicit finite difference approximation for Eq. (5) can be written as follows (see Ref. 4):

$$\sigma\bar{\delta}_\tau\left(\frac{\rho_{ij}^{n+1}}{J}\right) + \bar{\delta}_\xi\left\{\frac{\rho_{i+\frac{1}{2},j}^{n+1}}{J}\left[\sigma\xi_t^{n+1} + A_{1\,i+\frac{1}{2},j}^{n+1}\vec{\delta}_\xi\phi_{i+\frac{1}{2},j}^{n+1} + A_{2\,i+\frac{1}{2},j}^{n+1}\delta_\eta\phi_{i+\frac{1}{2},j}^{n}\right]\right\} + \bar{\delta}_\eta\left\{\frac{\rho_{i,j+\frac{1}{2}}^{n+1}}{J}\left[\sigma\eta_t^{n+1} + A_{2\,i,j+\frac{1}{2}}^{n+1}\delta_\xi\phi_{i,j+\frac{1}{2}}^{n} + A_{3\,i,j+\frac{1}{2}}^{n+1}\vec{\delta}_\eta\phi_{i,j+\frac{1}{2}}^{n+1}\right]\right\} = 0 \tag{8}$$

where U and V are expressed in terms of the usual metric components A_1, A_2, and A_3. Here, standard notation is used for the finite difference operators.

The spatially differenced quantities in Eq. (8) are evaluated at computational grid half-points. Thus, the computational module for this expression is a five-point star which includes contributions from grid points identified by the indices $(i-1,j)$, (i,j), $(i+1,j)$, $(i,j+1)$ and $(i,j-1)$. To preserve this five-point module, cross-derivative terms in the spatial directions (i.e., product terms such as $\delta_\xi\delta_\eta$) are lagged by one time step for unsteady problems, or by one relaxation cycle for steady flow cases.

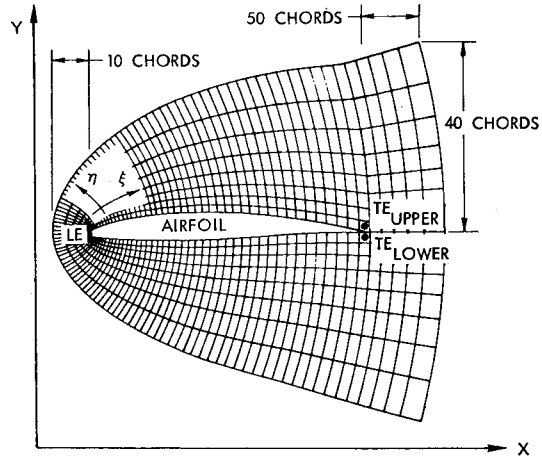

Fig. 1 Sheared parabolic numerical grid.

Equation (8) is highly nonlinear due to the presence of the density/velocity-potential product terms. However, for computational efficiency, a noniterative, single-step, implicit procedure for advancing the numerical solution between successive time levels (or relaxation cycles) is desired. Thus, following Goorjian,[4] a time linearization is first performed to eliminate the ρ^{n+1} terms in Eq. (8). A Taylor's expansion of the density term is formed as follows:

$$\rho^{n+1} = \rho^n + \left(\frac{\delta\rho}{\partial\tau}\right)\Delta\tau + \sigma(\Delta\tau^2) \tag{9}$$

The term $(\delta\rho/\delta\tau)$ is found by differentiating Eq. (6) with respect to time,

$$\frac{\partial\rho}{\partial\tau} = M_\infty^2\rho^{2-\gamma}\left[\phi_{\tau\tau} + (\phi_\xi\xi_t)_\tau + (\phi_\eta\eta_t)_\tau + A_1\phi_\xi\phi_{\xi\tau} + A_2(\phi_\eta\phi_{\xi\tau} + \phi_\xi\phi_{\eta\tau}) + A_3\phi_\eta\phi_{\eta\tau} + \frac{A_{1\tau}}{2}\phi_\xi^2 + A_{2\tau}\phi_\xi\phi_\eta + \frac{A_{3\tau}}{2}\phi_\eta^2\right] \tag{10}$$

Equation (10) has a quadratic nonlinearity that also must be eliminated in order to produce a linear system of algebraic equations. In discretizing Eq. (10), terms such as $(\phi_\xi^{n+1})^2$ have been approximated as

$$(\phi_\xi^{n+1})^2 = \phi_\xi^n\phi_\xi^{n+1}$$

and terms such as $\phi_\xi^{n+1}\phi_\eta^{n+1}$ as

$$\phi_\xi^{n+1}\phi_\eta^{n+1} = \tfrac{1}{2}(\phi_\xi^n\phi_\eta^{n+1} + \phi_\xi^{n+1}\phi_\eta^n)$$

Likewise, the density terms included in spatial derivatives are linearized with respect to the time variable; that is,

$$\rho_{i+\frac{1}{2},j}^{n+1} \simeq \rho_{i+\frac{1}{2},j}^{n} + 0(\Delta t)$$

Equation (8) is then recast into the following expression:

$$\sigma\bar{\delta}_\tau\left\{\frac{\rho_{ij}^n}{J} - \frac{\Delta\tau}{J}M_\infty^2(\rho_{ij}^n)^{2-\gamma}\left[\bar{\delta}_\tau(\bar{\delta}_\tau\phi_{ij}^{n+1}) + \bar{\delta}_\tau(\delta_\xi\phi_{ij}^{n+1}\xi_t^{n+1}) + \bar{\delta}_\tau(\delta_n\phi_{ij}^{n+1}\eta_t^{n+1}) + Q_1 + A_{1ij}^{n+1}\delta_\xi\phi_{ij}^n\bar{\delta}_\tau(\delta_\xi\phi_{ij}^{n+1}) + A_{2ij}^{n+1}\left[\delta_\eta\phi_{ij}^n\bar{\delta}_\tau(\delta_\xi\phi_{ij}^{n+1}) + \delta_\xi\phi_{ij}^n\bar{\delta}_\tau(\delta_\eta\phi_{ij}^{n+1})\right] + A_{3ij}^{n+1}\delta_\eta\phi_{ij}^n\bar{\delta}_\tau(\delta_\eta\phi_{ij}^{n+1})\right\} + \bar{\delta}_\xi\left\{\frac{\rho^n}{J^n}\left[\xi_t^{n+1} + A_1^{n+1}\vec{\delta}_\xi\phi^{n+1} + A_2^{n+1}\delta_\eta\phi^n\right]\Big|_{i+\frac{1}{2},j}\right\} + \bar{\delta}_\eta\left\{\frac{\rho^n}{J^n}\left[\eta_t^{n+1} + A_2^{n+1}\delta_\xi\phi^n + A_3^{n+1}\delta_\eta\phi^{n+1}\right]\Big|_{i,j+\frac{1}{2}}\right\} = 0 \tag{11}$$

Here the term Q_1 represents contributions due to time derivatives of the metric coefficients. The expression for Q_1 is written as

$$Q_1 = \tfrac{1}{2}\{\bar{\delta}_\tau(A_1^{n+1})[\delta_\xi\phi^n\delta_\xi\phi^{n+1}]\}|_{ij} + \tfrac{1}{2}\{\bar{\delta}_\tau(A_3^{n+1})[\delta_\eta\phi^n\delta_\eta\phi^{n+1}]\}|_{ij} + \tfrac{1}{2}\{\bar{\delta}_\tau(A_2^{n+1})[\delta_\xi\phi^{n+1}\delta_\xi\phi^n + \delta_\xi\phi^n\delta_\eta\phi^{n+1}]\}|_{ij} \tag{12}$$

where the derivative with respect to time operates only on the metric coefficients A_1, etc.

Equation (11) is next recast into correction form to reduce numerical roundoff error; that is,

$$\phi^{n+1} = \phi^n + \Delta\phi^{n+1} \tag{13}$$

where $\Delta\phi^{n+1}$ is the correction required to advance the solution between time steps, or, for steady flow problems, between consecutive relaxation cycles.

After substituting Eq. (13) into Eq. (11) and collecting terms, the final discretized system of equations in correction form can be written as a pentadiagonal matrix equation at each node point (i,j). A typical matrix row is given below.

$$B\Delta\phi^{n+1}_{i,j-1} + D\Delta\phi^{n+1}_{i-1,j} + E\Delta\phi^{n+1}_{i,j} + F\Delta\phi^{n+1}_{i+1,j} + H\Delta\phi^{n+1}_{i,j+1} = R^n \tag{14}$$

The finite difference expressions used to evaluate the terms B, D, E, F, H, and R^n in Eq. (14) are given in Ref. 9. Certain factors in these terms, which result from discretizing the unsteady term $(\rho/J)_\tau$ in the continuity equation, are written using windward finite differences. The use of windward differencing, while providing only first-order accurate contributions, nevertheless serves to increase the diagonal dominance of the resulting matrix equations, and hence contributes to the overall robustness of the solution procedure.

In regions of supersonic flow, an upwind bias must be added to the potential equation to simulate the physical zone of influence at each computational grid point. In the present work this upwind bias was applied through the artificial compressibility concept described by Holst and Albert.[10] For biasing in the ξ direction the following expression is used:

$$\tilde{\rho}_{ij} = \rho_{ij} + \mu_{ij}\tilde{\delta}_\xi \rho_{ij} \tag{15}$$

where

$$\mu_{ij} = C_1 \max[0,\ 1 - (M_c^2/M_{ij}^2)] \tag{16}$$

Here M_c is a cutoff Mach number, while M_{ij} is the local Mach number and C_1 is a user-defined constant. A similar expression is used for biasing in the η direction.

In steady flow cases only, provision is made for adding damping terms proportional to $\phi_{\xi\tau}$ and $\phi_{\eta\tau}$ to the left-hand side of Eq. (14). This artificial damping is added only in supersonic regions. Since these terms tend to slow convergence, a constant multiplicative factor is used to eliminate or magnify these damping terms as the case may warrant.

Simple averages are used to compute most quantities required at grid half-points. However, for values of density required at these points, the half-nodes are used as recommended by Hafez et al.[11] In addition, a binomial expansion is used to eliminate the requirement for exponentiation in computing fluid densities. For transonic cases, the midpoint density formulation tends to reduce shock overshoots. Also, experience with the sheared parabolic grid described in the next section shows that the use of midpoint densities produces smoother density gradients in the regions of rapid grid slope change along lines that emanate from the airfoil trailing edge.

Computational Grid

For the present work, solutions to Eq. (14) were computed on a body-fitted, sheared parabolic grid. During unsteady solutions, the computational grid is rotated and/or translated rigidly with the airfoil. This moving grid system is used to facilitate application of the appropriate boundary conditions at locations on the instantaneous airfoil surface.

The sheared parabolic grid is formed by unwrapping about a singularity point embedded near the leading edge of the airfoil. The airfoil wake is assumed to lie along a cut starting at the airfoil trailing edge and extending approximately 50 chords in the downstream direction. Along the upstream direction, the wraparound grid extends approximately 10 chord lengths in front of the airfoil leading edge. Finally, in the lateral direction, the computational grid expands from a height of 10 chords above and below the airfoil to a height of 40 chords on either side of the wake cut at the far downstream boundary. A typical grid is shown in Fig. 1.

For airfoils which include trailing-edge flaps, a second shearing of the wraparound grid is made downstream of the flap hinge location. The flap rotation is approximated by a vertical translation of all grid points aft of the hinge point. As discussed by Steger and Bailey,[12] this grid generation method eliminates grid line crossover. Only a small change in the total airfoil chord results from this approximation for realistic flap deflections.

Currently, two grid systems are utilized for steady flow solutions: A coarse grid containing 847 grid points (77×11) with 52 points around the airfoil surface, and a fine grid with 3213 grid points (153×21) of which 104 points lie on the airfoil surface. Grid sequencing is used for steady flow problems to increase the convergence rate of the solution procedure. At present, unsteady computations are performed only on the fine grid.

Implementation of Boundary Conditions

The matrix system of equations represented by Eq. (14) is sovled for each interior node point on the computational grid. Boundary conditions along the coordinate line adjacent to the airfoil surface and wake are used to modify the computational module corresponding to this matrix row prior to solution of the equations. Then, after the velocity potential is updated everywhere in the interior domain, similar boundary conditions are used to update the potential along the airfoil surface and wake cut.

Along the airfoil surface, the matrix row in Eq. (14) is rewritten as

$$D\Delta\phi^{n+1}_{i-1,2} + \left[\frac{4}{3}B + E\right]\Delta\phi^{n+1}_{i,2} + F\Delta\phi^{n+1}_{i+1,2} + \left[H - \frac{1}{3}B\right]\Delta\phi^{n+1}_{i,3}$$

$$= R^n + \frac{2}{3}B(\phi^n_{\eta i,1} + 1.5\phi^n_{i,1} - 2.0\phi^n_{i,2} + 0.5\phi^n_{i,3}) \tag{17}$$

where second-order accurate, one-sided differencing has been used to arrive at Eq. (17). An expression for the current value of the derivative of ϕ, with respect to η at the surface of the airfoil, is obtained using the tangential flow boundary condition, $V=0$. Then,

$$V|_{i,1} = [n_t^{n+1} + A_2^{n+1}\phi^n_\xi + A_3^{n+1}\phi^n_\eta]\,|_{i,1} = 0$$

or

$$\phi^n_{\eta i,1} = [-(\eta_t^{n+1} + A_2^{n+1}\phi^n_\xi)/A_3^{n+1}]\,|_{i,1} \tag{18}$$

Along the wake cut the effects of the wake boundary condition on the interior points are lagged in order to preserve a pentadiagonal system of equations. Equation (14) is then written as before with $\Delta\phi_{i,1} = 0$ downstream of the trailing edge.

After the correction matrix has been determined throughout the flowfield, the velocity potential on the airfoil surface is updated using the following second-order accurate expression:

$$\phi^{n+1}_{i,1} = \frac{4}{3}\phi^{n+1}_{i,2} - \frac{1}{3}\phi^{n+1}_{i,3} - \frac{2}{3}\left[\frac{-\eta_t^{n+1} - A_2^{n+1}\phi^n_\xi}{A_3^{n+1}}\right]\Bigg|_{i,1} \tag{19}$$

For unsteady flows, the wake potentials are updated by solving the linearized vorticity propagation equation

$$\Gamma_t + U\Gamma_\xi = 0 \tag{20}$$

where Γ is the jump in potential across the wake. A backward difference in x is used to implement Eq. (20). This leads to a simple marching scheme which is initialized at the airfoil trailing edge. For steady flows, $\delta t = 0$, and a second-order accurate, one-sided differencing algorithm is used to update the velocity potential along the wake.

Freestream conditions are enforced along the outer boundaries. A compressible vortex solution is added to the freestream potential for both steady and unsteady flow problems; that is,

$$\phi_{\text{far field}} = \phi_\infty + \frac{\Gamma}{2\pi} \tan^{-1}\left(\sqrt{1-M_\infty^2}\,\frac{y}{x}\right) \tag{21}$$

where

$$\phi_\infty = x\cos\alpha_m + y\sin\alpha_m \tag{22}$$

and α_m is the mean angle of attack of the airfoil. For unsteady flow problems, the freestream potential is recomputed at each time step to account for grid motion changes to the values of x and y in Eq. (22). For unsteady flows, the value of Γ corresponding to the starting solution is used in Eq. (21).

Approximate Factorization Procedure

Stone's[13] strongly implicit procedure is used to solve Eq. (14). Since Stone's method operates on the discretized equations, such as Eq. (14), both the steady and unsteady forms of the full-potential equation can be solved with the same solution algorithm. In addition, Stone's method has the desirable property of matrix conditioning; that is, it automatically adjusts the diagonals of the matrix solution so that they are always well conditioned both in regions where the mesh spacing is small and in regions where mesh spacing is large. Complete discussions of Stone's method can be found in Refs. 13-15 and, therefore, only a limited discussion of the method will be made here.

Equation (14) represents a system of simultaneous equations for the quantity $\Delta\phi^{n+1}$ at all interior points, and this system may be written formally as

$$[M]\{\Delta\phi\}^{n+1} = \{R\}^n \tag{23}$$

Stone's method converts the matrix $[M]$ into a new matrix $[M]'$ which can be inverted easily and is, in some sense, close to the original matrix. Using Stone's procedure, $[M]'$ is split into an upper and lower triangular matrix pair so that

$$[L][U] = [M]' \simeq [M] \tag{24}$$

Simple recursion equations are then used to solve for the desired correction vector.

Stone's approximate factorization method incorporates a relaxation parameter α. For steady flow problems, α is varied according to the following relationship in the present calculations:

$$\alpha = 1.0 - (0.001)^{n/N}, \qquad n = 0,1,\ldots,N \tag{25}$$

where N is the maximum number of elements in the α sequence. Note that in the above sequence α varies between 0 and 0.999 cyclically. The strongly implicit procedure is not overly sensitive to the sequence of α values used. For example, a sequence of values between 0 and 0.95 would work just as well. Stone has indicated, based on a von Neumann analysis, that larger values of α tend to suppress the low-frequency components of error in the solution and vice versa. For time-dependent flow problems, α is always set to unity in order to minimize the added error terms.

For steady, fluid dynamic problems, the sweep direction of the recursion relationships does not seem to significantly effect the convergence rate of the algorithm. However, Stone's LU decomposition is derived by using a Taylor series

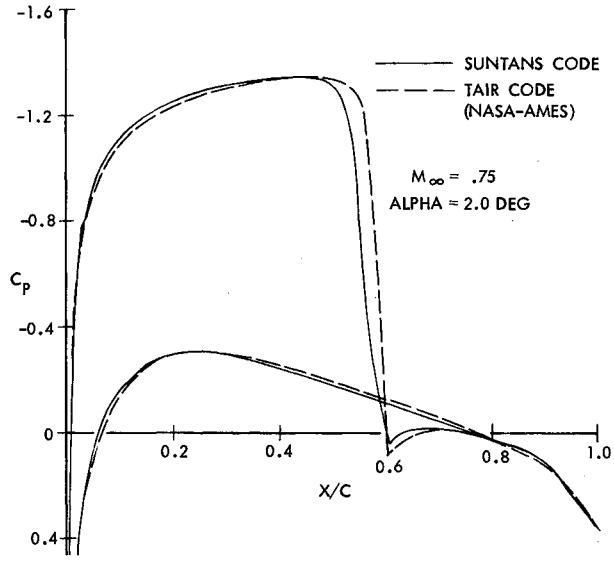

Fig. 2 Computed surface pressure distributions on NACA 0012 airfoil.

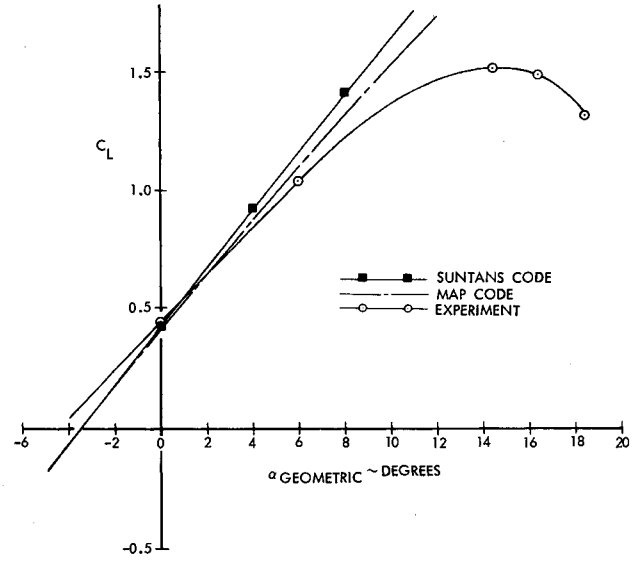

Fig. 3 Calculated and measured lift coefficients for GA(W)-1 airfoil.

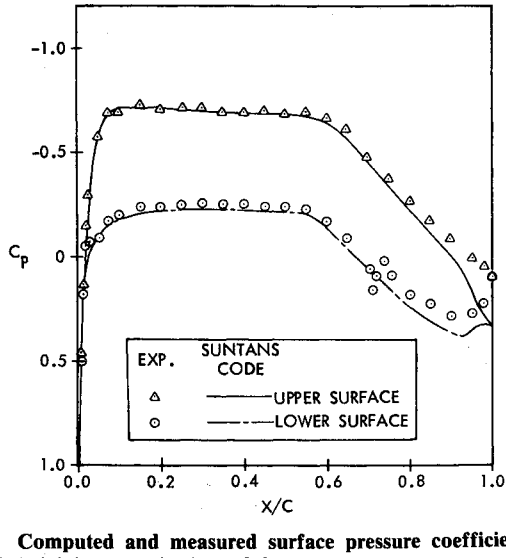

Fig. 4 Computed and measured surface pressure coefficients for GA(W)-1 airfoil, $M_\infty = 0.14$, $\alpha = 0$ deg.

expansion which is asymmetric with respect to the original five-point computation module at each grid node point. For unsteady flows, the authors have found it necessary to alternate sweep directions in the ξ direction in order to achieve symmetrical flows in certain cases. Since changing sweep directions does not increase the computational effort, the authors use this technique for all flow problems, both steady and unsteady. The interested reader can see Pepper and Harris[16] for details of the recursion equations used in the present solution procedure.

Results and Discussion

A computer program has been written to solve the two-dimensional, full-potential equation using the algorithm described in the previous sections. The computer code, which will be referred to here as SUNTANS (steady and unsteady transonic airfoil numerical solutions). can be used to compute steady or unsteady flows about arbitrary airfoil shapes.

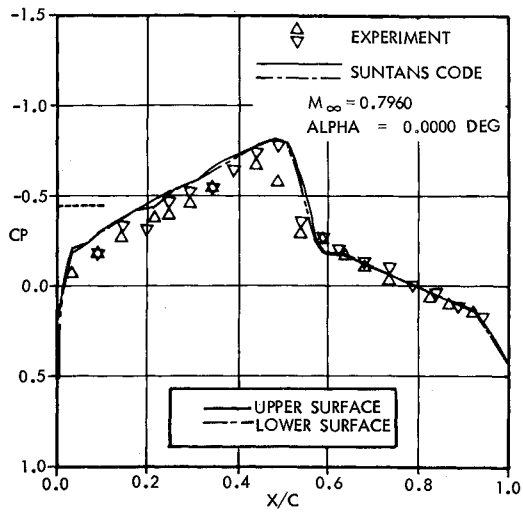

Fig. 5 Computed and measured surface pressure coefficients for NACA 64A010 airfoil, $M_\infty = 0.796$, $\alpha = 0$ deg.

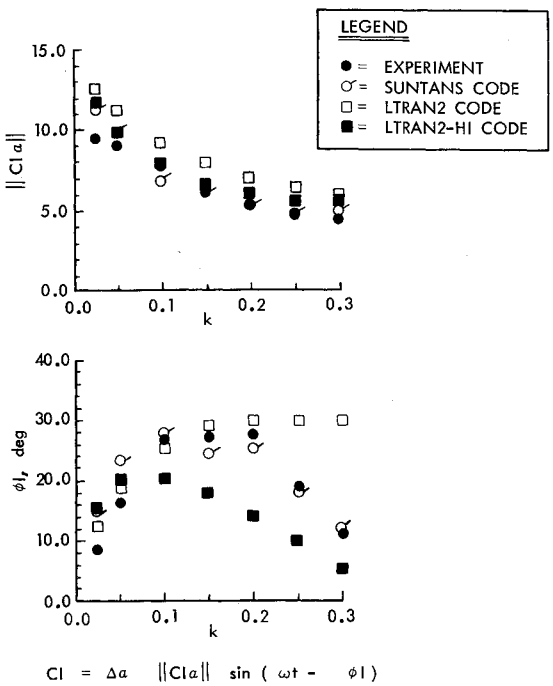

Fig. 6 Unsteady lift coefficient vs reduced frequency for NACA 64A010 airfoil.

Sample results for both steady and unsteady flows are presented to illustrate the capabilities of this computer program.

A standard number of relaxation iterations was used for most of the steady flow cases presented here. This sequence (400 coarse, 600 fine grid iterations) has been shown to provide converged solutions, even for quite difficult transonic flow cases. As a comparison, subcritical solutions normally would require fewer than 100 fine grid iterations. The multiplicative constant used for the upwind density biasing was set to 1.0 for most steady cases and 2.0 for unsteady flows. The metric terms A_1, A_2, and A_3 that appear in Eq. (5) were evaluated using fourth-order finite difference formulas.

NACA 0012 Airfoil

Figure 2 shows the computed surface pressure distribution for an NACA 0012 airfoil in steady transonic flow. The Mach number for this case is 0.75 and the angle of attack is 2.0 deg. A comparison is made with a pressure distribution obtained from the two-dimensional, steady transonic flow code, TAIR.[10] Although each code uses a different grid system (TAIR uses an "O" grid) and a different solution algorithm, the correlation of surface pressure distributions is quite reasonable. There is good agreement between upper and lower surface peak suction values. The shock location and computed shock jumps are comparable.

GA(W)-1 Airfoil

The current version of the SUNTANS code can be used to compute aerodynamic flows over a wide Mach number range

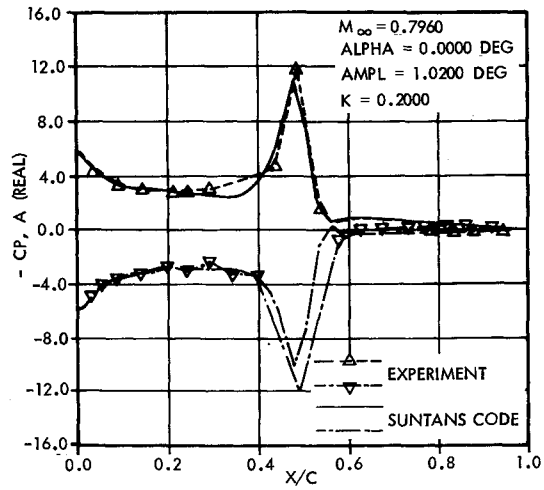

Fig. 7 Real component of unsteady surface pressure coefficients for NACA 64A010 airfoil.

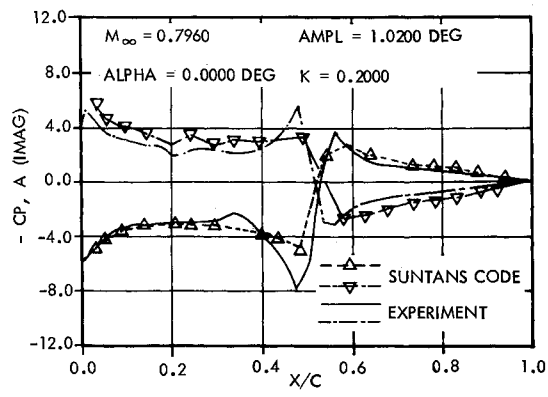

Fig. 8 Imaginary component of unsteady surface pressure coefficients for NACA 64A010 airfoil.

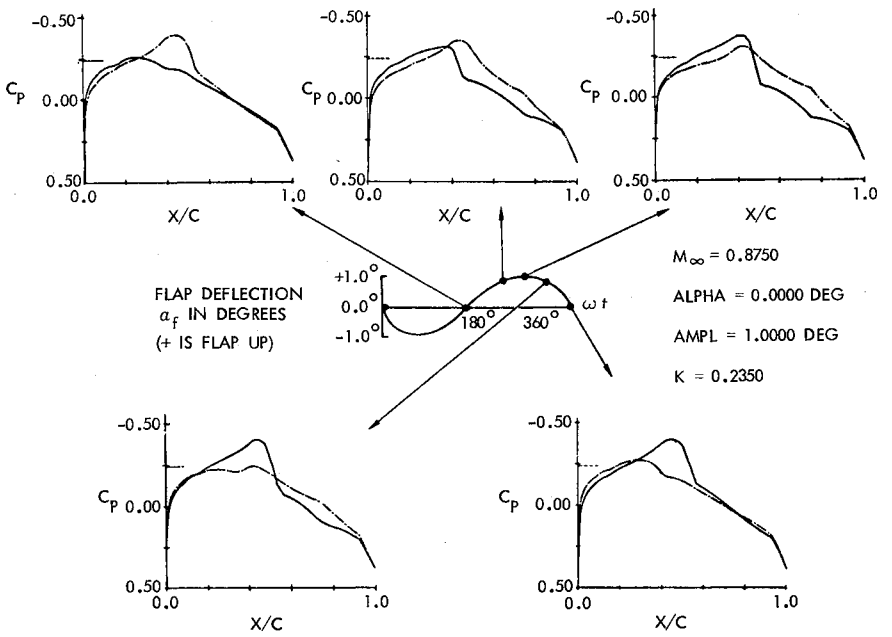

Fig. 9 Time histories of surface pressures on NACA 64A006 airfoil with oscillating flap.

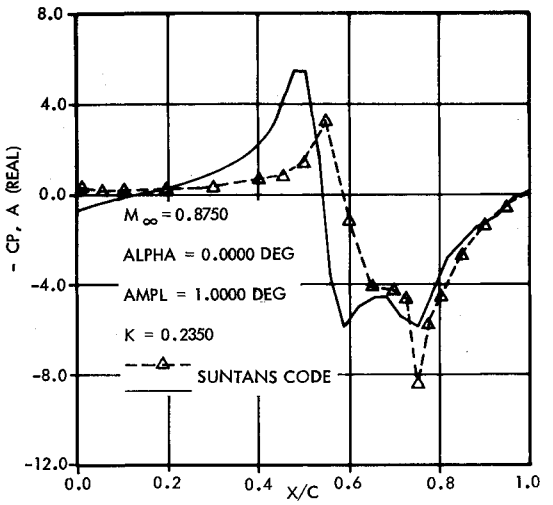

Fig. 10 Real component of unsteady surface pressure coefficients for NACA 64A006 airfoil with oscillating flap.

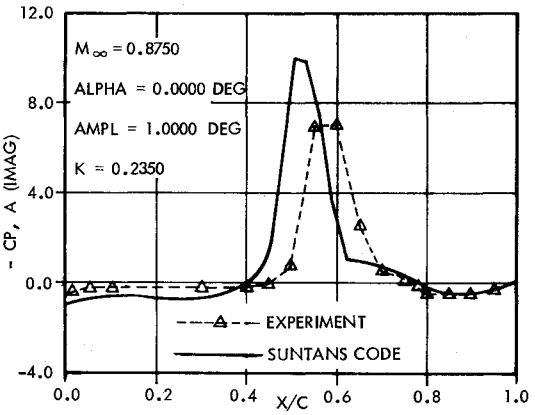

Fig. 11 Imaginary component of unsteady surface pressure coefficients for NACA 64A006 airfoil with oscillating flap.

($0.1 < M < 1.0$). Figure 3 presents computed lift coefficients for the GA(W)-1 airfoil at a low subsonic speed, $M_\infty = 0.14$. Also shown on this figure are experimental data measured at Wichita State University and numerical results from a multiple-element airfoil, viscous flow panel method (MAP). The full-potential results were computed for the geometric test angles of 0, 4, and 8 deg. Angle-of-attack corrections were not required here to obtain good correlation with experiment at $\alpha = 0$ deg. Some amount of angle-of-attack correction, however, would be needed to account for viscous or blockage effects at the higher lift coefficients.

Pressure coefficient distributions for both the airfoil upper and lower surfaces are shown in Fig. 4 for the $\alpha = 0$ case. Also given in the figure are experimental data for the corresponding tunnel conditions.

NACA 64A010 Airfoil

Figure 5 compares computed and measured steady flow surface pressure distributions for the NACA 64A010 airfoil. The experimental pressure distributions were obtained from Ref. 17. The test Mach number is 0.796 and the test angle of attack is −0.21 deg. The numerical results from the SUNTANS code are presented for the same test Mach number, but an angle of attack of 0 deg. The correlation of upper and lower surface shock locations, and pressure distributions aft of the shock position is excellent. The suction pressures on the forward portion of the airfoil, however, are somewhat overpredicted.

Figures 6-8 show results of unsteady flow computations for the NACA 64A010 airfoil undergoing sinusoidal pitching oscillations about the quarter-chord. The freestream Mach number was 0.796 and the amplitude of oscillation was 1.02 deg.

Unsteady calculations were made for seven different values of reduced frequency, with k ranging between 0.025 and 0.3 based on semichord. A Fourier series analysis was made of airfoil pressure coefficient distributions, lift, and leading-edge moment coefficients corresponding to the fourth cycle of airfoil oscillation. Figure 6 shows the magnitude and phase angle of the first harmonic component of the airfoil lift coefficient. Also shown in the figure are the corresponding experimental[18] data and similar numerical results previously presented by Hessenius and Goorjian.[19] Moment coefficient results can be found in Ref. 9.

Figures 7 and 8 show the real and imaginary components of the airfoil pressure coefficient distribution corresponding to a reduced frequency of 0.2. The full-potential results are compared with the experimental data of Ref. 18. The theory/test correlation is better for the real component of

pressure, since the magnitude of the imaginary component is somewhat underpredicted over the airfoil chord. However, the shock-wave trajectory and mean position are seen to be predicted adequately.

NACA 64A006 Airfoil

Figures 9-11 show computational results for an NACA 64A006 airfoil fitted with an oscillating trailing-edge flap. The freestream Mach number is 0.875, while the mean airfoil and flap incidences are each 0 deg. The flap hinge line is located at the airfoil 75% chord position. For this unsteady calculation, the flap deflection was oscillated sinusoidally between ± 1 deg at a reduced frequency of 0.235 based on airfoil semichord.

Figure 9 shows a sequence of upper and lower surface pressure distributions at five different times during the flap oscillation cycle. The experimentally measured type B shock motion, in which the shock wave disappears during a portion of the flap cycle, is seen to be predicted by the full-potential theory. Figures 10 and 11 compare theory and experiment[19] for the real and imaginary components of the airfoil surface pressure coefficient.

Computer Requirements

The SUNTANS code was originally developed for use on a VAX 11/780 computing facility. Liberal use has been made of the virtual core memory capability of this computer. Typical computing times for the code are: 23 min for a 1000-iteration steady flow relaxation solution; 120 min for a 1440 time-step unsteady solution. This represents a 25% increase in computational resources over a VAX version of the NASA Ames LTRAN2 code which is currently operational at Lockheed-Georgia (50% increase on a per-grid-point basis). The increased analysis capability provided by the full-potential formulation, however, presently justifies the increased computation resources required to execute the code. Since the present version of the code is not optimized for the VAX system, the authors feel that a reasonable reduction in computational execution run times is possible. One area of improvement would be the elimination of unnecessary computer system page faults by appropriate modifications to program coding.

Concluding Remarks

A numerical procedure has been developed for solving steady and unsteady, two-dimensional, subsonic or transonic potential flows in a body-fitted coordinate system. The numerical results obtained thus far indicate that the present method can be used either as a relaxation procedure or as a noniterative time-marching procedure. The present method should prove to be a useful tool for aerodynamic and aeroelastic analysis of arbitrary airfoil sections.

References

[1]Lores, M. E., Smith, P. R., and Hicks, R. M., "Supercritical Wing Design Using Numerical Optimization and Comparisons with Experiment," AIAA Paper 79-0065, Jan. 1979.

[2]Garner, H. C. and Lehrian, E. E., "Comparative Theoretical Calculations of Forces on Oscillating Wings Through the Transonic Speed Range," ARC R&M 3559, 1969.

[3]Steger, J. L. and Caradonna, F. X., "A Conservative Implicit Finite Difference Algorithm for the Two-Dimensional Unsteady Transonic Full Potential Equation," NASA TM 81211, 1980.

[4]Goorjian, P. M., "Implicit Computations of Unsteady Transonic Flow Governed by the Full Potential Equation in Conservative Form," AIAA Paper 80-0150, Jan. 1980; also, NASA CR-152274, June 1979.

[5]Chipman, R. and Jameson, A., "An Alternating-Direction Implicit Algorithm for Unsteady Potential Flow," *AIAA Journal*, Vol. 20, Jan. 1982, pp. 18-24.

[6]Sankar, N. L. and Tassa, Y., "An Algorithm for Unsteady Transonic Potential Flow Past Airfoils," *Seventh International Conference on Numerical Methods in Fluid Dynamics Proceedings*, Stanford University, June 1980, pp. 367-372.

[7]Chang, I. C., "Unsteady Transonic Flow Past Airfoils in Rigid Body Motion," Courant Institute of Mathematical Sciences, New York University, New York, R&D Rept. DOE/ER/03077-170, March 1981.

[8]Bridgeman, J. O., Steger, J. L., and Caradonna, F. X., "A Conservative Finite Difference Algorithm for the Unsteady Transonic Potential Equation in Generalized Coordinates," AIAA Paper 82-1388, Aug. 1982.

[9]Malone, J. B. and Sankar, N. L., "Numerical Simulation of 2-D Unsteady Transonic Flows Using the Full-Potential Equation," AIAA Paper 83-0233, Jan. 1983.

[10]Holst, T. L. and Albert, J., "An Implicit Algorithm for the Conservative, Transonic Full-Potential Equation with Effective Rotated Differencing," NASA TM 78570, April 1979.

[11]Hafez, M., South, J., and Murman, E., "Artificial Compressibility Methods for Numerical Solutions of Transonic Full Potential Equations," *AIAA Journal*, Vol. 17, Aug. 1979, pp. 838-844.

[12]Steger, J. L. and Bailey, H. E., "Calculation of Transonic Aileron Buzz," *AIAA Journal*, Vol. 18, March 1980, pp. 249-255.

[13]Stone, H. L., "Iterative Solution of Implicit Approximations of Multi-Dimensional Partial Differential Equations," *SIAM Journal of Numerical Analysis*, Vol. 5, No. 3, 1968, pp. 530-538.

[14]Sankar, N. L., Malone, J. B., and Tassa, Y., "A Strongly-Implicit Procedure for Steady Three-Dimensional Transonic Potential Flow," *AIAA Journal*, Vol. 20, May 1982, pp. 598-605.

[15]Sankar, N. L., Malone, J. B., and Tassa, Y., "An Implicit Conservative Algorithm for Steady and Unsteady Three-Dimensional Transonic Potential Flows," AIAA Paper 81-1016, June 1981.

[16]Pepper, D. W. and Harris, S. D., "Fully Implicit Algorithms for Solving Partial Differential Equations," *Journal of Fluids Engineering*, Vol. 99, Dec. 1977, pp. 781-783.

[17]Davis, S. S. and Malcolm, G. N., "Experimental Unsteady Aerodynamics of Conventional and Supercritical Airfoils," NASA TM 81221, Aug. 1980.

[18]Olsen, J. J., et al., "Compendium of Unsteady Aerodynamic Measurements," AGARD Rept. 702, Aug. 1982.

[19]Hessenius, K. A. and Goorjian, P. M., "A Validation of LTRAN2 with High Frequency Extensions by Comparisons with Experimental Measurements of Unsteady Transonic Flows," NASA TM 81307, July 1981.